ELSEVIER

Contents lists available at ScienceDirect

Science Bulletin

journal homepage: www.elsevier.com/locate/scib



Article

Observation of D-class topology in an acoustic metamaterial

Shi-Qiao Wu ^{a,b,c,1}, Wenting Cheng ^{d,1}, Xiao-Yu Liu ^a, Bing-Quan Wu ^a, Emil Prodan ^{e,*}, Camelia Prodan ^{f,*}, Jian-Hua Jiang ^{a,g,*}

- a School of Physical Science and Technology & Collaborative Innovation Center of Suzhou Nano Science and Technology, Soochow University, Suzhou 215006, China
- ^b School of Physics and Optoelectronic Engineering, Foshan University, Foshan 528000, China
- ^c Guangdong-Hong Kong-Macao Joint Laboratory for Intelligent Micro-Nano Optoelectronic Technology, Foshan University, Foshan 528000, China
- ^d Department of Physics, University of Michigan, Ann Arbor MI 48109, USA
- ^e Department of Physics, Yeshiva University, New York NY 10033, USA
- ^f Department of Physics and Engineering Physics, Fordham University, New York NY 10023, USA
- ⁸ Suzhou Institute for Advanced Research, University of Science and Technology of China, Suzhou 215123, China

ARTICLE INFO

Article history: Received 3 November 2023 Received in revised form 27 December 2023 Accepted 24 January 2024 Available online 1 February 2024

Keywords: D-class topology Chiral symmetry Time-reversal symmetry Particle-hole symmetry Gapless edge states

ABSTRACT

Topological materials and metamaterials opened new paradigms to create and manipulate phases of matter with unconventional properties. Topological D-class phases (TDPs) are archetypes of the ten-fold classification of topological phases with particle-hole symmetry. In two dimensions, TDPs support propagating topological edge modes that simulate the elusive Majorana elementary particles. Furthermore, a piercing of π -flux Dirac-solenoids in TDPs stabilizes localized Majorana excitations that can be braided for the purpose of topological quantum computation. Such two-dimensional (2D) TDPs have been a focus in the research frontier, but their experimental realizations are still under debate. Here, with a novel design scheme, we realize 2D TDPs in an acoustic crystal by synthesizing both the particle-hole and fermion-like time reversal symmetries for a wide range of frequencies. The design scheme leverages an enriched unit cell structure with real-valued couplings that emulate the targeted Hamiltonian of TDPs with complex hoppings: A technique that could unlock the realization of all topological classes with passive metamaterials. In our experiments, we realize a pair of TDPs with opposite Chern numbers in two independent sectors that are connected by an intrinsic fermion-like timereversal symmetry built in the system. We measure the acoustic Majorana-like helical edge modes and visualize their robust topological transport, thus revealing the unprecedented D and DIII class topologies with direct evidence. Our study opens up a new pathway for the experimental realization of two fundamental classes of topological phases and may offer new insights in fundamental physics, materials science, and phononic information processing.

© 2024 Science China Press. Published by Elsevier B.V. and Science China Press. All rights reserved.

1. Introduction

The discovery of topological insulators and related topological phases of matter [1–5] has permanently revolutionized our understanding of materials. With the inclusion of topological superconductors and topological semimetals, topological states of matter form a large family of materials with exotic properties. In this family of materials, symmetry plays a pivotal role in their emergent physical effects. It has been conjectured [6,7] that there are three fundamental symmetries and combinations thereof that can stabilize boundary modes that are immune to Anderson localization.

This led to the ten-fold classification of strong topological insulators and superconductors [7]. Earlier, Altland and Zirnbauer [8] have shown that the normal and superconducting mesoscopic systems fall into ten and only ten distinct classes that can also be distinguished by fundamental symmetries. It turns out that these classes predicted and characterized by Altland and Zirnbauer can be sampled, at least in principles, by the boundary modes of the topological states from the ten-fold classification table, or by the bulk metallic states emerging at the topological phase transitions (see, e.g., Ref. [9] for numerical demonstrations). In addition to these fundamental characteristics, each topological phase from the ten-fold table enables unique physics effects, such as the helical topological edge modes in the AlI and DIII class, the stabilization of the Majorana zero-dimensional modes by π -flux piercings in D-class systems, and the emergence of a solid-state analog of

^{*} Corresponding authors.

E-mail addresses: prodan@yu.edu (E. Prodan), cprodan@fordham.edu (C. Prodan), ijanhuajjang@suda.edu.cn (I.-H. Ijang).

¹ These authors contributed equally to this work.

Majorana particles at the edge boundaries of the D and DIII-class topological superconductors [10]. For these reasons, exploring topological states of matter in various symmetry classes is one of the major goals in the study of topological materials [11]. However, up till now, not all symmetry classes have been realized in experiments, which is by far still a vigor challenge in the research frontier.

Historically, around the time when the ten-fold table was perfected, topological phases were predicted for classical waves as well. For instance, topological Chern insulators, i.e., A-class topological insulators featured with unidirectional chiral edge states, were predicted for electromagnetic [12] and mechanical [13] systems. With the advantages in fabrication, tunability, and measurement, classical wave systems are becoming a rising force in the study of topological phenomena and their applications (see, e.g., [14–30]). For instance, it was proposed theoretically [13] and realized experimentally [14] that, with external driving, a mechanical system exhibits a Chern insulator phase. A mechanical analog of a quantum spin-Chern insulator (i.e., an AII-class topological insulator with additional U(1) symmetry) was later realized using smartly-designed couplings in a lattice of coupled pendula [15]. Other topological phases such as topological semimetals [31–37], higher-order topological insulators [38-41], fragile topological insulators [42], Kitaev chains [43], were realized in mechanical systems as well. However, as evidenced by the recent review articles [11,16–20], with decades of efforts, several fundamental topological classes, for instance, the topological D and DIII classes in dimension two and higher, remain outside the reach of experimental realizations, neither in condensed matter systems [11] nor in classical waves [16–20] (see Table 1). In superconductors, the topological D class corresponds to $p_x + ip_y$ superconductors that support chiral Majorana edge modes. The experimental discovery of such a topological matter has been under debate for years [44].

Here, we fill this gap by realizing 2D TDPs with acoustic metamaterials. The key features of TDPs are the non-trivial bulk topology and the underlying particle-hole symmetry. TDPs from the DIII class have the additional feature of a fermionic time reversal symmetry. These symmetries are very difficult to achieve in the existing forms of metamaterials [16-20] because they are anti-unitary and have to be enforced over a substantial window of frequencies. Here, we exploit an unconventional approach to overcome such a challenge and realize an acoustic TDP with pseudospin-polarized Chern number ± 1 . Our solution here is based on lattice models of coupled acoustic cavities with enriched unit-cell structures, where a projected symmetry of a subset of bands can simulate any targeted symmetries, covering all ten symmetry classes [45]. Such a scheme can generate the exact combinations of symmetries as well as the topology of the bands needed for the TDP, with a design based only on real-valued couplings. This design has the advantage of intrinsic broad band couplings that realize the targeted symmetries without fine tuning. With such a design, we realize the acoustic TDP with gapless topological edge modes that exhibit the particle-hole symmetry. Using acoustic pump-probe measurements, we directly observe the Majorana-like topological edge modes of the TDP and visualize the robust one-dimensional (1D) topological sound transport along the edge boundaries.

2. Methods

2.1. Numerical simulations

All simulations of acoustic wave dynamics and calculation of acoustic energy bands were conducted by using acoustic pressure module of the commercial finite-element solver COMSOL Multiphysics. Due to the huge acoustic impedance mismatch between

air and the photosensitive resin used in the 3D printing and transparent hoses composing of polyvinyl chloride, the latter two constituents can be treated as sound hard boundaries in numerical simulation. Sound waves encapsulated inside the sample propagate in the air with a mass density 1.23 kg/m³ and a speed 343 m/s at room temperature (around 20 °C). The bulk dispersion relations of the acoustic waves in the 2D sonic crystal are calculated based on a primitive lattice with the Floquet Bloch boundary conditions imposed on the edge boundaries in both x- and y-directions and sound hard boundary conditions on the other boundaries. To calculate the projected bands of the ribbonshaped supercell, the system is set as periodic in x-direction but finite in y-direction with ten primitive cells. Specifically, to obtain the acoustic pressure maps in finite lattice, point source was fixed at the bottom-right sites of the sample with frequencies in the bulk band gap.

2.2. Experimental measurements

Every column of sample along y direction was manufactured by 3D printing technology using photosensitive resin and was assembled layer-by-layer along x direction. Due to the huge complexity of coupling between the nearest neighboring unit cells and the precision of 3D printing machine, our experimental sample cannot be fabricated as a whole directly. Soft tube composing of polyvinyl chloride with identical length can facilitate the couplings of different cavities and it is also hard enough for acoustic wave to be regarded as closed boundaries in simulation. To measure the acoustic pressure, a headphone of a diameter of 6 mm is utilized for acoustic excitations with the frequency sweeping from 0.5 to 1.2 kHz at a step of 1 Hz. The headphone is placed and enclosed in the top cavity of the sample to excite corresponding eigenstates. A tiny microphone is connected with the network analyzer (Keysight E5061B) and inserted into each cavity of the upper layer to detect the acoustic pressure. Such measurements contain both the amplitude and phase profiles of the acoustic pressure field, thanks to the data processing by the network analyzer (i.e., the Fourier transformation of the real-time acoustic signal). Through fast Fourier transformations of the detected acoustic pressure profiles in real-space at each pump-probe frequency, we map the detected signals to wavevector-frequency space which are then compared with the simulated acoustic dispersions in the sample. The signal in the wavevector-frequency space is essentially the spectral functions of the acoustic phonons in the system. In our experiments, we perform such measurements on the sample edge and compare the acoustic spectral functions with the simulated acoustic dispersions of the edge states.

3. Results

3.1. Theoretical model

While the minimal representative lattice models for each class in the periodic table of topological insulators and superconductors are well known [7], most of these lattice models, in particular those corresponding to the TDPs, contain complex hopping terms. In acoustic crystals, such complex couplings can be implemented with finely tailored acoustic bridges, but such a design works only at a single frequency. This is unacceptable in the present context because the symmetries of topological phases need to be implemented over a broad range of frequencies for both the bulk and edge states. Our design principle here rests on the observation that complex couplings can be emulated with real-valued couplings if the degrees of freedom are doubled [45]. Specifically, this goal is achieved by replacing the imaginary unit i = $\sqrt{-1}$ with the matrix

Table 1Topological symmetry classes in two-dimensional (2D) systems^a.

Topological class	Time-reversal symmetry	Particle-hole symmetry	Chiral symmetry	Realization in 2D metamaterials
A	0	0	0	√ [14,30]
D	0	+1	0	×
DIII	-1	+1	1	×
AII	-1	0	0	√ [15,27]
C	0	-1	0	×

^a There are five nontrivial topological classes in 2D systems, characterized by combinations of time-reversal, particle-hole, and chiral symmetries. The number 0 in each column stands for absence of symmetry, while ± 1 indicate the presence of a symmetry together with the even or odd character of the symmetry operator relative to squaring. The check marks in the last column indicate whether the topological symmetry class has been realized in 2D metamaterials in the past, and citations to the relevant works are placed next to the marks.

$$\begin{pmatrix} 0 & 1 \\ -1 & 0 \end{pmatrix}$$
. This substitution maps any complex tight-binding

Hamiltonian $H = \sum \hat{t}_{r,r'}c_r^{\dagger}c_{r'}$ (with c_r^{\dagger} and $c_{r'}$ denoting the creation and annihilation operators for the local degrees of freedom r and r', respectively) of the targeted topological symmetry class to a real-valued Hamiltonian H', by expanding the hopping matrices $\hat{t}_{r,r'}$ as

$$\widehat{\boldsymbol{t}}_{\boldsymbol{r},\boldsymbol{r}'} \to \widehat{\boldsymbol{\chi}}_{\boldsymbol{r},\boldsymbol{r}'} = \begin{pmatrix} \operatorname{Re}(\widehat{\boldsymbol{t}}_{\boldsymbol{r},\boldsymbol{r}'}) & \operatorname{Im}(\widehat{\boldsymbol{t}}_{\boldsymbol{r},\boldsymbol{r}'}) \\ -\operatorname{Im}(\widehat{\boldsymbol{t}}_{\boldsymbol{r},\boldsymbol{r}'}) & \operatorname{Re}(\widehat{\boldsymbol{t}}_{\boldsymbol{r},\boldsymbol{r}'}) \end{pmatrix}. \tag{1}$$

Therefore, if H has N degrees of freedom in each unit cell and $\widehat{t}_{r,r'}$ are $N \times N$ matrices, then H' has 2N degrees of freedom in each unit cell and $\widehat{\chi}_{r,r'}$ are $2N \times 2N$ matrices. As this mapping preserves all the algebraic relations, H and H' thus have the same spectrum, but the spectrum of H' is doubly degenerate due to the doubling of the degrees of freedom. Moreover, the bulk-boundary correspondence is preserved as well: If H with a boundary displays topological edge modes, so does H'. A crucial observation is that the Hamiltonian H' with real-valued coupling matrices can serve as the dynamical matrix of a passive mechanical metamaterial, which can be implemented by placing 2N resonators in each unit cell and by engineering their couplings according to Eq. (1) [45].

Regarding the symmetries of such mechanical systems, we point out that such dynamical matrices automatically commute with $U = \begin{pmatrix} 0 & \mathbb{I} \\ -\mathbb{I} & 0 \end{pmatrix}$ (\mathbb{I} is the $N \times N$ identity matrix) and hence T = UK is a symmetry operator (K is the complex conjugation operator). Therefore, a so-designed mechanical system has a built-in fermion-like time reversal symmetry $T^2 = U^2 = -1$ and Kramers degeneracy at all time-reversal invariant momenta, a feature that is required for the DIII class. Our realization of the fermion-like time-reversal symmetry is similar to that in Ref. [15] but different from the approaches based on crystalline symmetries [27,41]. In the latter cases, the Kramers degeneracy can be realized only in one or a portion of the time-reversal invariant momenta. The matrix U has two eigenvalues, $\pm i$, which divide the phononic spectrum of the mechanical system into two independent sectors that are invariant by the dynamics of phonons, and the projections onto these sectors are denoted as Π_{+} . One sector is mapped into the other by the fermion-like time reversal symmetry [45]. It was revealed theoretically that the projected Hamiltonians $\Pi_+ H' \Pi_+$ onto each of these sectors have the same set of symmetries as the targeted Hamiltonian [45,46] (see the Supplementary materials). Yet these two sectors carry opposite Chern numbers, as they are the fermion-like time-reversal counterparts of each other.

In our case, we choose the following targeted Hamiltonian to be the minimal model for the D-class in two dimensions [7]

$$H = it \sum_{j=1,2} \sigma_j \bigotimes \left(S_j - S_j^{\dagger} \right) + \sigma_3 \bigotimes \left[m + t \sum_{j=1,2} \left(S_j + S_j^{\dagger} \right) \right], \tag{2}$$

where σ_j 's (j=1,2,3) representing the x, y, and z directions, separately) are the Pauli matrices. $S_j = \sum_{r} c^{\dagger}_{r+a_j} c_r$ are the translation by the primitive lattice vector \mathbf{a}_j (j=1,2) in the square lattice. t and m are the hopping and Dirac mass parameters, respectively. It has the particle-hole symmetry implemented by the anti-unitary operator Θ_{PH} with Θ^2_{PH} =1. The phase diagram of this Hamiltonian and the associated topological edge states can be calculated analytically [46]. Transforming into the wavevector space, the above Hamiltonian becomes,

$$H(\mathbf{k}) = 2t\sin(k_x a)\sigma_x + 2t\sin(k_y a)\sigma_y + \left[m + 2t\cos(k_x a) + 2t\cos(k_y a)\right]\sigma_z, \tag{3}$$

where a is the lattice constant. This model, which is also known as the Qi-Wu-Zhang model [5], exhibits two nontrivial gapped phases with Chern numbers $C = \operatorname{sgn}(m)$ if |m| < 4t, a trivial gapped phase with Chern number C = 0 for |m| > 4t, and topological transition points at m = 0 and $m = \pm 4t$ (see the Supplementary materials). The topologically gapped phase, in the context of topological superconductors, supports gapless Majorana edge states with particle-hole symmetry [46]. The procedure explained above supplies out of H a real-valued dynamical matrix H' with four degrees of freedom per unit cell, displaying a fermion-like time reversal symmetry implemented by the operator $\begin{pmatrix} 0 & I_2 \\ -I_2 & 0 \end{pmatrix} \mathcal{K}$ and a particle-hole symmetry operator $\Theta_{PH} = \begin{pmatrix} 0 & \sigma_x \\ \sigma_x & 0 \end{pmatrix} \mathcal{K}$, where I_2 is the 2 × 2 identity

matrix. Therefore, H' belongs to the DIII class and such mechanical system will support topological edge states that are the classical analog of the helical Majorana edge states in time-reversal invariant topological superconductors. Moreover, due to the built-in fermion-like symmetry, the projected dynamical matrices $\Pi_{\pm}H'\Pi_{\pm}$ each realize a D-class topological phase which can be observed and manipulated independently in the laboratory.

We remark that, as our system consists of two independent sectors of D-class topological phases with opposite Chern numbers, the final outcome resembles a DIII class topological phase. It should be pointed out that, however, as the two sectors are independent, the essential topological physics is the same as that of the D-class topological phases. This scenario is like a topological insulator consists of two independent copies of quantum anomalous Hall systems with opposite Chern numbers as the schematics illustrated in Fig. 1a. Such a topological insulator seems like a quantum spin Hall insulator but is essentially different, as this topological phase is essentially the same as the quantum anomalous Hall insulators. In comparison, the quantum spin Hall insulator is characterized by different topology where the spin-orbit coupling and the Kramers degeneracy play a key role.

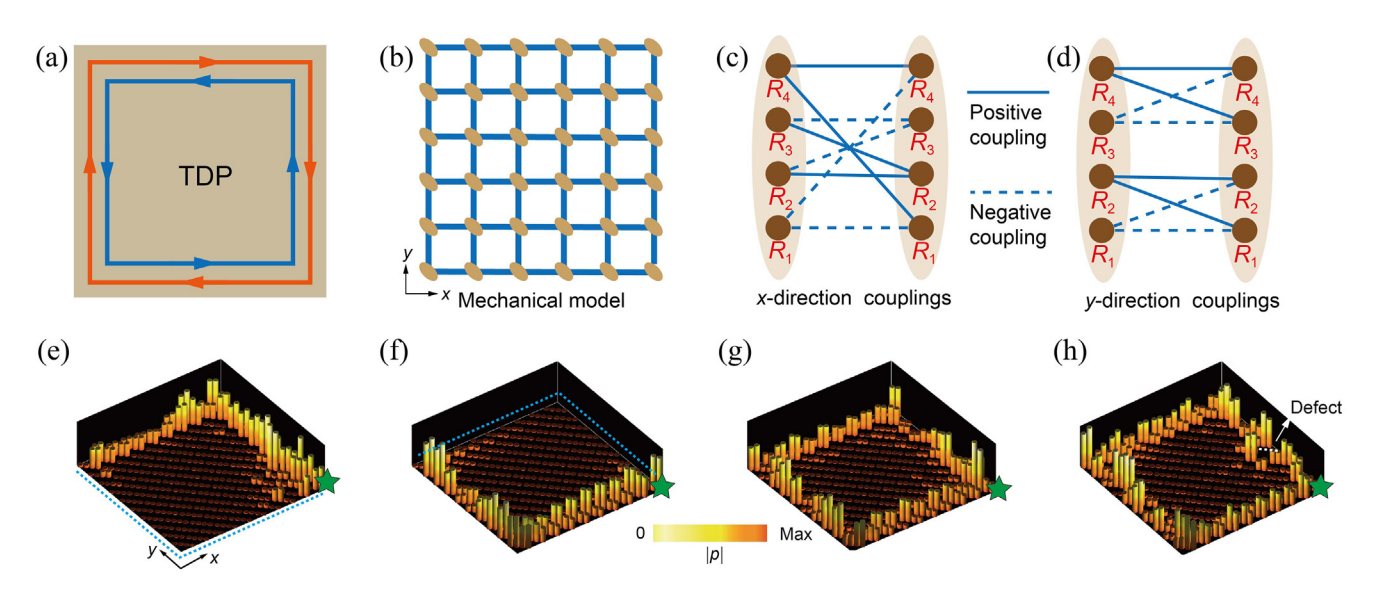


Fig. 1. (Color online) A TDP realized with an acoustic platform. (a) Schematic of a TDP from DIII-class with a doubled symmetry representation and hosting two branches of counter-propagating Majorana-like topological edge states. (b) Schematic of the mechanical model that implements the TDP, realized on a square-lattice acoustic metamaterial. Each site (orange ellipse) consists of four acoustic resonators (R_1 , R_2 , R_3 , and R_4) that are coupled together in a designed way (blue lines), as illustrated in (c) and (d). (c) gives the couplings in the x direction, while (d) for the y direction. All couplings are of the same strength. (e)—(h) Robust topological transport of sound in the acoustic TDP at different boundary conditions as calculated from full-wave simulations. (e) and (f) Half-open boundaries where the open edge boundaries are indicated by the blue dotted lines. (g) Close boundary condition without defect. (h) Close boundary condition with a defect. In (e)—(h) acoustic waves are excited by a point source (green star) with a frequency in the topological band gap (around 840 Hz). The dissipation of acoustic waves is not included in the simulations.

3.2. Acoustic metamaterial design

The couplings of the mechanical resonators, as derived from the mapped Hamiltonian H', are illustrated in Fig. 1b—d. As seen in Fig. 1c and d, each resonator has eight couplings of equal strength with the neighboring resonators, but they are positive as well as negative. By realizing these couplings with coupled acoustic cavities, we arrive at an acoustic crystal supporting TDPs with robust topological sound transport at the edges, as evidenced by the COMSOL simulation results in Fig. 1e—h. Specifically, these simulations show that the edge states can propagate both clockwise and counterclockwise without backscattering: a key feature of the helical edge states (Fig. 1e and f). Furthermore, the topological edge waves can propagate around a defect, showing robustness of the topological sound transport. These properties, together with the results shown in Fig. 2, demonstrate the effectiveness of our approach in simulating various topological classes.

Using the above design, we fabricate the acoustic topological crystal with the commercial 3D printing technology based on photosensitive resins. The unit-cell structure of the acoustic crystal and the fundamental acoustic modes are depicted in Fig. 2a and b. The fabricated sample with 10×10 unit-cells is shown in Fig. 2c. To realize both the positive and negative couplings sketched in Fig. 1c and d, we design the H-shaped acoustic cavities. As shown in Fig. 2b, in these cavities the first resonating mode has uniform pressure field along the long arms, but the two arms have opposite acoustic pressures. The positive and negative couplings between the H-shaped cavities are then realized by the in-phase and outof-phase couplings via short acoustic bridges, respectively (Fig. 2b). The other advantage of the design here is that the bridges can be attached to four ends, reducing the load per end. Moreover, the strength of each coupling is determined by the length of the acoustic bridge which is the same for all couplings in our system to realize the model in Eq. (2).

With four H-shaped resonators, R_1 , R_2 , R_3 , and R_4 , in a unit-cell, we achieve the couplings sketched in Fig. 1c and d to realize the targeted Hamiltonian in Eq. (2). The constant mass term in Eq. (2) is realized by the difference in the first resonating mode

frequency of the H-shaped cavities enabled by tuning the height of the resonators (Fig. 2b). Specifically, R_1 and R_3 have a height h_2 , while R_2 and R_4 have a height h_1 , and $m \propto (h_1 - h_2)$. The geometric parameters are as follows: The lattice constant of the square lattice is a=80 mm. The diameter of the long arms of the H-shaped cavity is $d_1=22$ mm. The two long arms have a center-to-center distance of $l_1=27$ mm, while the tube connecting them has a diameter $d_2=3$ mm. The heights of the H-shaped resonators are chosen as $h_1=57.8$ mm and $h_2=62.2$ mm. All couplings between the H-shaped resonators are realized by soft tubes of the same length 120 mm and the same diameter $d_3=2$ mm. These soft tubes are glued to the 3D-printed framework of the H-shaped cavities. The synthetic symmetries and band topology of the acoustic crystal are analyzed in detail in the Supplementary materials.

Based on the above design, full-wave simulations based on COMSOL Multiphysics give the acoustic bulk band structure (Fig. 2d) comparable with the tight-binding band structure (Fig. 2e) generated with the couplings from Fig. 1c and d. Note that, in acoustic systems, we solve the acoustic wave equation, and the eigenvalues have the meaning of resonant frequency square, which is to be compared with the tight-binding energy. In addition, the band structure (Fig. 2d) should be referenced from the middle of the acoustic band gap occurring at the finite angular frequency square $2.8\times10^7~{\rm rad}^2/{\rm s}^2$. The acoustic bands show a notable spectral symmetry with respect to the mid-gap angular frequency square: A sign of the successful realization of the particle-hole symmetry in acoustic systems.

Experimentally, we use the pump-probe technique to measure the Majorana-like acoustic edge modes. Here, the edge modes are excited with an acoustic source (a tiny speaker) inserted in a cavity at the edge boundary with the excitation frequency in the bulk band gap. Meanwhile, an acoustic detector (a small microphone) is inserted into another cavity at the edge boundary to probe the acoustic signal in that cavity. A network analyzer is used to track the detected acoustic signal at the excitation frequency. As the network analyzer Fourier transforms the time-resolved acoustic signal, the measurement gives both the amplitude and the phase of the

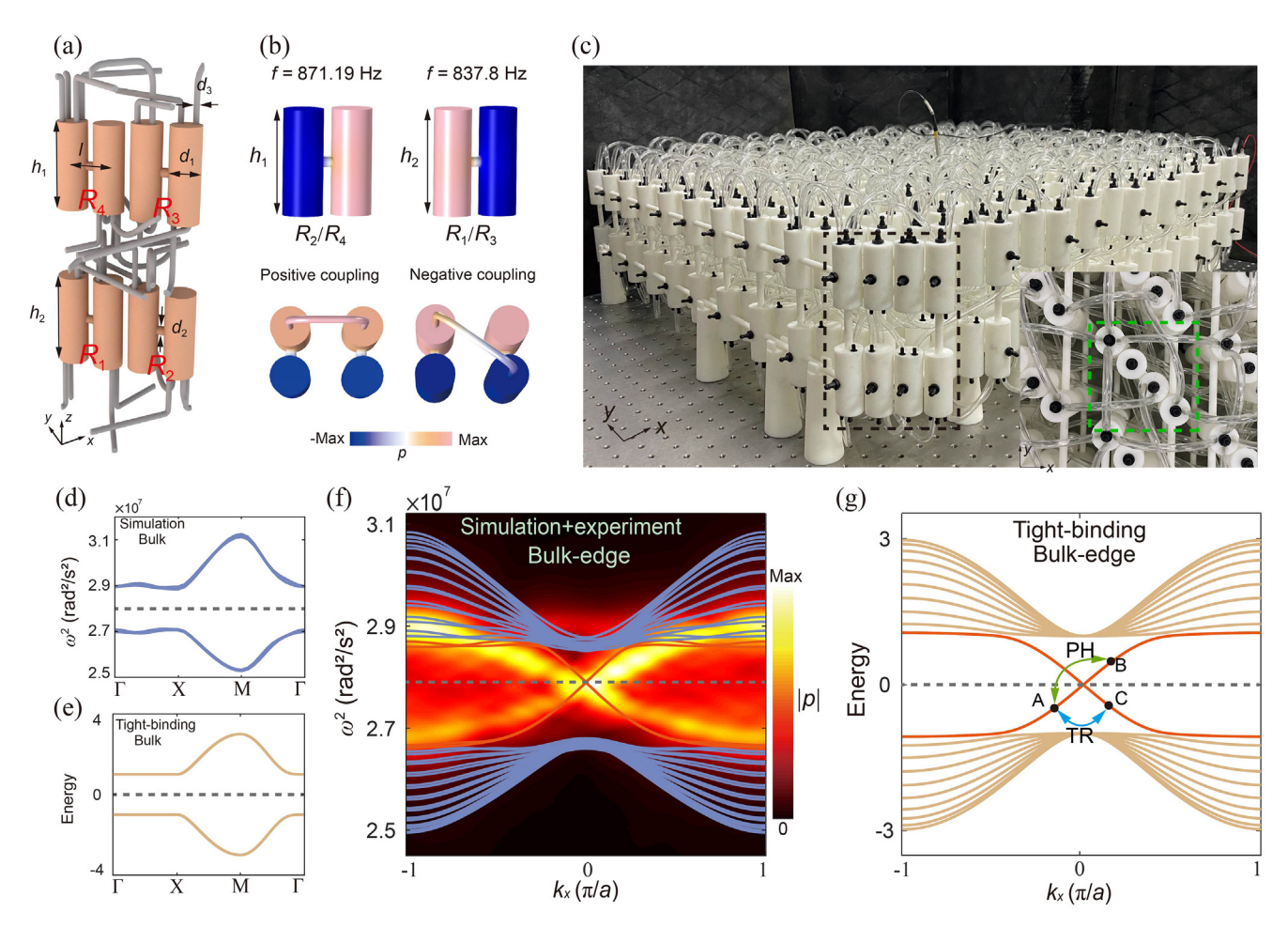


Fig. 2. (Color online) Observation of the Majorana-like helical edge states in the acoustic TDP. (a) Specific design of the acoustic metamaterial using H-shaped acoustic resonators (orange) and the short-bridge couplings (gray) among them. (b) The first acoustic resonating modes in the H-shaped resonators and the realization of the positive and negative couplings. The color scheme represents the acoustic pressure (i.e., the acoustic wave amplitude). (c) A photo of the experimental system. The main part of the bilayer acoustic metamaterial is fabricated by the 3D printing technology based on resins. Couplings between resonators are realized by soft tubes. Black plugs are used to facilitate the insertion of the tiny speaker (source) and microphone (detector) which are connected to a network analyzer. Inset: Zoom-in top-view of the system. The black dashed box (main) and the green dashed box (inset) indicate a unit-cell. (d) Simulated bulk acoustic bands. (e) Bulk bands from the tight-binding model with m = 1 and t = -0.5. (f) Measured and simulated acoustic dispersions at the edge boundary. (g) Calculated acoustic dispersions at the edge boundary from the tight-binding model. Note the tight-binding model here refers to the model depicted in Fig. 1c and d. Here A, B, and C label three edge states that are connected with each other via the particle-hole (PH) symmetry and the time-reversal (TR) symmetry. Dashed lines in (d), (e) and (g) label the mid-gap frequency square, while in (f) it labels the frequency square of the Dirac point.

pump-probe signal (see Methods and the Supplementary materials for details). By measuring the distribution of the pump-probe signal and Fourier transforming the signal from spatial to wavevector dependence, the acoustic edge spectrum is obtained (Fig. 2f) which is consistent with both the simulation and tight-binding calculation (Fig. 2g). These results show excellently the emergence of gapless topological edge states in the acoustic band gap, confirming an important signature of the TDP. Moreover, both the bulk and edge spectra are nearly symmetric around the mid-gap. The Dirac point in the edge band is at $2.78\times10^7~{\rm rad}^2/{\rm s}^2$ which is very close to the mid-gap angular frequency square of the bulk. Small deviation between the experiments and the simulation for the edge bands may originate from the intrinsic acoustic dissipation.

We remark that in Fig. 2f slight lift of the Kramers degeneracy at $k_x = \frac{\pi}{a}$ can be noted which is due to the long-range hoppings that are almost unavoidable in acoustic metamaterials. These unwanted additional hoppings make the acoustic dispersion deviates from the ideal tight-binding model slightly. Consequently, the Kramers degeneracy at $k_x = \frac{\pi}{a}$ is lifted a little bit. Nevertheless, such degeneracy lifting is still negligible and much smaller than in pre-

vious realizations of fermion-like time-reversal symmetry based on the crystalline symmetry [27,41].

The topological edge band is constrained by the synthetic particle-hole and time-reversal symmetries, as illustrated in Fig. 2g. These constraints dictate that an edge band necessarily crosses the mid gap point an odd number of times and such crossing can only be at the k=0 or $k=\pi$. For our acoustic crystal, this crossing happens at k = 0, as shown in Fig. 2f. Moreover, these edge bands must have zero curvature when they cross the middle of the bulk band gap due to these symmetry constraints. This vanishing curvature implies that a wave packet excited around the mid-gap will exhibit no deformation. Therefore, such wavepacket will propagate very much like a massless particle traveling along the edge of the sample with a speed given by the slope of the edge band at k = 0, thus excellently emulating the elusive Majorana elementary particle. This phenomenon, which though cannot be tested in our system due to the small size, can be verified in future systems with much larger size.

A direct manifestation of the unique band topology and the above symmetry features is the robust dynamics of the acoustic

edge waves. For this purpose, we measure the acoustic wave propagation in and outside the topological band gap in our sample (a top-view scheme is given in Fig. 3a). By selectively exciting only one symmetry sector of the acoustic edge states in the topological band gap, we can achieve unidirectional acoustic wave propagation in both the clockwise and anticlockwise directions (Fig. 3b and c). The results show that the acoustic edge waves can perfectly turn around the sample corner without noticeable back reflection. In sharp contrast, when the excitation frequency is outside the topological band gap, the excited acoustic wave propagates in all directions in the sample (Fig. 3d). A careful quantitative examination on the wave amplitude along the propagation channels (either edge or bulk) shows that the acoustic edge waves propagate steadily along the edge channels in a unidirectional way for each sector, except an overall decay due to the intrinsic dissipation of the acoustic waves (Fig. 3e and f). In comparison, the bulk acoustic

wave spreads out in all directions (Fig. 3g). More details and discussion on the dissipation effect can be found in the Supplementary materials.

We now test the robustness of the topological edge channel for acoustic wave propagation by introducing defects in the edge channel (Fig. 4a). In conventional 1D acoustic waveguides, such defects cause severe backscattering which substantially reduces the performance of the acoustic waveguides [16]. In contrast, in our acoustic TDP, even when a notable defect is introduced at the edge boundary by removing one unit-cell, the acoustic wave still propagates steadily along the edge channel (Fig. 4b and c). This stable wave dynamics in the edge channel is indicated when both the clockwise and anticlockwise edge modes are excited or when only one of them is excited. In both these cases, the acoustic wave propagates perfectly around the defect. A careful look at the quantitative measurement of the acoustic wave amplitude along the

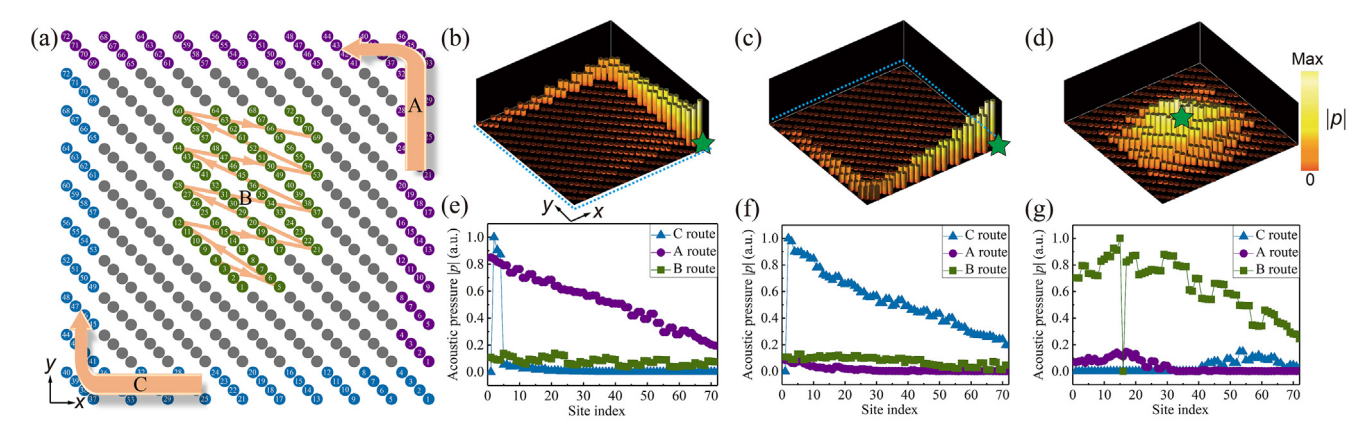


Fig. 3. (Color online) Observation of topological edge transport in the acoustic TDP. (a) Schematic top-view of the lattice structure of the acoustic metamaterial. Numbers label the sites where the edge waves and bulk waves propagate through which will be used in (e)-(g). (b) Transport of sound along the anticlockwise edge when the left and lower edge boundaries are open (indicated by the blue dotted lines). (c) Transport of sound along the clockwise edge when the right and upper edge boundaries are open (indicated by the blue dotted lines). (d) Transport of sound in the bulk. (e)-(g) Acoustic pressure, i.e., the sound wave amplitude, along three transport paths: The anticlockwise edge path (A route), the clockwise edge path (C route), and the bulk path (B route) at different conditions. (e) The same condition as in (b) with an excitation frequency 842.2 Hz. (f) The same condition as in (d) with an excitation frequency 875 Hz.

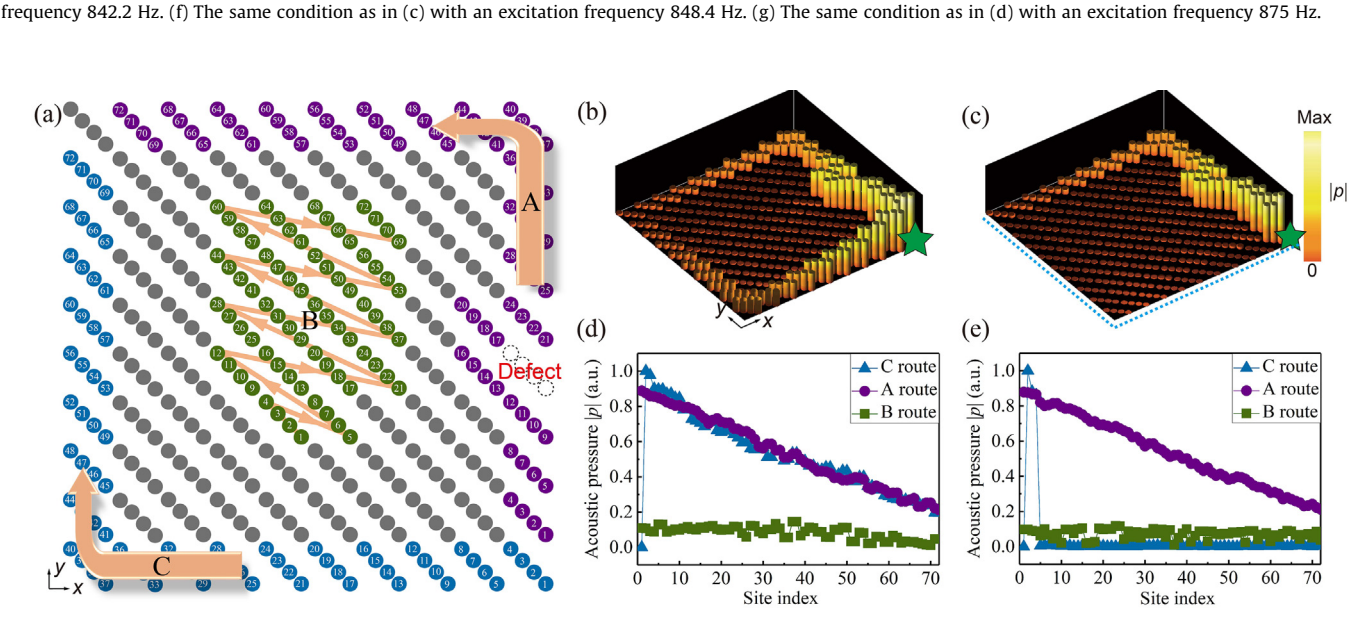


Fig. 4. (Color online) Visualizing robust topological transport of sound in acoustic TDP. (a) Schematic top-view of the lattice structure of the acoustic metamaterial with a defect introduced by removing four cavities (dashed ones at the right edge). Numbers label the sites where the edge waves and bulk waves propagate through which will be used in (d) and (e). (b) Topological sound transport along the edges with closed edge boundaries and the defect (excitation frequency 844 Hz). (c) Topological sound transport along the anticlockwise edge path with the defect where the left and lower edge boundaries (dashed blue lines) are open (excitation frequency 840 Hz). (d), (e) The acoustic wave amplitude along the clockwise (C route) and anticlockwise (A route) edge paths as well as along the bulk path (B route) for the condition corresponding to (b) and (c), respectively.

edge channels also confirms the stable wave propagation (Fig. 4d and e): In Fig. 4d, the acoustic wave amplitudes along both the clockwise and anticlockwise routes are comparable, despite that the acoustic edge wave along the anticlockwise path encounters the defect quickly after it is excited. This is strong evidence that the defect does not disturb the acoustic wave propagation in the edge channel. Fig. 4e confirms the robustness of the edge wave dynamics again by the stable unidirectional wave propagation. In particular, the acoustic wave amplitude does not have any notable change when propagating around the defect and the corner of the sample. These careful observations indicate signatures of a strong topological insulator phase.

4. Discussions and outlook

Our study unveils a new type of topological metamaterials supporting D- and DIII-class topological phases, which are featured with a combination of synthetic particle-hole and fermionic time reversal symmetries. With acoustic pump-probe measurements, we verified the existence of the expected topological helical edge states in our acoustic TDP and demonstrated the robust topological sound transport in the edge channels. Our technique for realizing TDPs with metamaterials made of passive elements offers a powerful platform for materialization of various topological symmetry classes, including those that have not yet been realized so far (Table 1).

Furthermore, the realization of TDPs can enable Majorana-like local modes stabilized by π -fluxes. As demonstrated in Refs. [47,48], the braiding and fusion of π -fluxes are non-trivial and worth exploring even at the one-particle level covered by the linear wave equation regime employed here. We mention that, in one dimension, the work on Majorana-like modes implemented with classical degrees of freedom is vigorously underway, particularly with the recent work [43,49–54] demonstrating the experimental control at a fascinating level that makes the classical systems feasible for information storage and processing. In 2D acoustic systems, implementing the π -fluxes will require nonuniform perturbations of the couplings which will be an important direction in the future.

Conflict of interest

The authors declare that they have no conflict of interest.

Acknowledgments

Jian-Hua Jiang thanks the support from the National Key R&D Program of China (2022YFA1404400), the National Natural Science Foundation of China (12125504 and 12074281), the Gusu Leading Innovation Scientists Program of Suzhou City, and the Priority Academic Program Development (PAPD) of Jiangsu Higher Education Institutions. Shi-Qiao Wu acknowledges the support from the National Natural Science Foundation of China (12047541) and the Research Fund of Guangdong-Hong Kong-Macao Joint Laboratory Intelligent Micro-Nano Optoelectronic (2020B1212030010). Wenting Cheng and Camelia Prodan acknowledge support from the US National Science Foundation (CMMI-2131759). Emil Prodan acknowledges support from the US National Science Foundation (DMR-1823800 and CMMI-2131760) and the U. S. Army Research Office through contract W911NF-23-1-0127.

Author contributions

Jian-Hua Jiang, Camelia Prodan, and Emil Prodan guided the research. Wenting Cheng, Camelia Prodan, and Emil Prodan estab-

lished the theory. Wenting Cheng, and Shi-Qiao Wu designed the system and performed simulations. Shi-Qiao Wu, Xiao-Yu Liu, and Bing-Quan Wu performed the experiments. All the authors contributed to the discussions of the results and the manuscript preparation. Jian-Hua Jiang, Camelia Prodan, Emil Prodan, Shi-Qiao Wu, and Wenting Cheng wrote the manuscript.

Appendix A. Supplementary materials

Supplementary materials to this article can be found online at https://doi.org/10.1016/j.scib.2024.01.041.

References

- [1] Kane CL, Mele EJ. Z₂ topological order and the quantum spin Hall effect. Phys Rev Lett 2005;95:146802.
- [2] Bernevig BA, Hughes TL, Zhang SC. Quantum spin Hall effect and topological phase transition in HgTe quantum wells. Science 2006;314:1757–61.
- [3] König M, Wiedmann S, Brüne C, et al. Quantum spin Hall insulator state in HgTe quantum wells. Science 2007;318:766–70.
- [4] Hasan MZ, Kane CL. Colloquium: Topological insulators. Rev Mod Phys 2010;82:3045–67.
- [5] Qi XL, Zhang SC. Topological insulators and superconductors. Rev Mod Phys 2011;83:1057–110.
- [6] Schnyder AP, Ryu S, Furusaki A, et al. Classification of topological insulators and superconductors in three spatial dimensions. Phys Rev B 2008;78:195125.
- [7] Ryu S, Schnyder AP, Furusaki A, et al. Topological insulators and superconductors: Tenfold way and dimensional hierarchy. New J Phys 2010;12:65010.
- [8] Altland A, Zirnbauer MR. Nonstandard symmetry classes in mesoscopic normal-superconducting hybrid structures. Phys Rev B 1997;55:1142–61.
- [9] Prodan E. A Computational Non-Commutative Geometry Program for Disordered Topological Insulators. Berlin: Springer; 2017.
- [10] Chiu CK, Teo JCY, Schnyder AP, et al. Classification of topological quantum matter with symmetries. Rev Mod Phys 2016;88:035005.
- [11] Wieder BJ, Bradlyn B, Cano J, et al. Topological materials discovery from crystal symmetry. Nat Rev Mater 2022;7:196–216.
- [12] Haldane FDM, Raghu S. Possible realization of directional optical waveguides in photonic crystals with broken time-reversal symmetry. Phys Rev Lett 2008:100:013904.
- [13] Prodan E, Prodan C. Topological phonon modes and their role in dynamic instability of microtubules. Phys Rev Lett 2009;103:248101.
- [14] Nash LM, Kleckner D, Read A, et al. Topological mechanics of gyroscopic metamaterials. Proc Natl Acad Sci USA 2015;112:14495–500.
- [15] Süsstrunk R, Huber SD. Observation of phononic helical edge states in a mechanical topological insulator. Science 2015;349:47–50.
- [16] Ma G, Sheng P. Acoustic metamaterials: from local resonances to broad horizons. Sci Adv 2016;2:e1501595.
- [17] Ozawa T, Price HM, Amo A, et al. Topological photonics. Rev Mod Phys 2019;91:015006.
- [18] Xue H, Yang Y, Zhang B. Topological acoustics. Nat Rev Mater 2022;7:974–90.
- [19] Ni X, Yves S, Krasnok A, et al. Topological metamaterials. arXiv:2211.10006, 2022.
- [20] Zhu W, Deng W, Liu Y, et al. Topological phononic metamaterials. Rep Prog Phys 2023;86:06501.
- [21] Wang Z, Chong Y, Joannopoulos JD, et al. Observation of unidirectional backscattering immune topological electromagnetic states. Nature 2009;461:772–5.
- [22] Rechtsman MC, Zeuner JM, Plotnik Y, et al. Photonic Floquet topological insulators. Nature 2013;496:196–200.
- [23] Khanikaev AB, Hossein Mousavi S, Tse WK, et al. Photonic topological insulators. Nat Mater 2013;12:233–9.
- [24] Yang Z, Gao F, Shi X, et al. Topological acoustics. Phys Rev Lett 2015;114:114301.
- [25] Peng YG, Qin CZ, Zhao DG, et al. Experimental demonstration of anomalous Floquet topological insulator for sound. Nat Commun 2016;7:13368.
- [26] Xiao M, Chen WJ, He WY, et al. Synthetic gauge flux and Weyl points in acoustic systems. Nat Phys 2015;11:920–4.
- [27] He C, Ni X, Ge H, et al. Acoustic topological insulator and robust one-way sound transport. Nat Phys 2016;12:1124–9.
 [28] Lu J, Qiu C, Ye L, et al. Observation of topological valley transport of sound in
- sonic crystals. Nat Phys 2017;13:369–74. [29] Prodan E, Dobiszewski K, Kanwal A, et al. Dynamical Majorana edge modes in a
- broad class of topological mechanical systems. Nat Common 2017;8:14587. [30] Ding Y, Peng Y, Zhu Y, et al. Experimental demonstration of acoustic Chern
- insulators. Phys Rev Lett 2019;12:014302.

 [31] Li F, Huang X, Lu J, et al. Weyl points and Fermi arcs in a chiral phononic
- crystal. Nat Phys 2017;14:30-4. [32] Yu SY, Sun XC, Ni X, et al. Surface phononic graphene. Nat Mater
- [32] Yu St, Sun XC, Ni X, et al. Surface phononic graphiene. Nat Mate 2016;15:1243-7.
- [33] He H, Qiu C, Ye L, et al. Topological negative refraction of surface acoustic waves in a Weyl phononic crystal. Nature 2018;560:61–4.

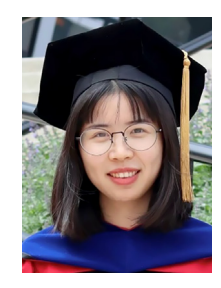
[34] Yang Y, Hx S, Jp X, et al. Topological triply degenerate point with double Fermi arcs. Nat Phys 2019;15:645–9.

- [35] Luo L, Wang HX, Lin ZK, et al. Observation of a phononic higher-order Weyl semimetal. Nat Mater 2021;20:794–9.
- [36] Wei Q, Zhang X, Deng W, et al. Higher-order topological semimetal in acoustic crystals. Nat Mater 2021;20:812–7.
- [37] Jiang B, Bouhon A, Lin ZK, et al. Experimental observation of non-Abelian topological acoustic semimetals and their phase transitions. Nat Phys 2021:17:1239-46.
- [38] Serra-Garcia M, Peri V, Süsstrunk R, et al. Observation of a phononic quadrupole topological insulator. Nature 2018;555:342-5.
- [39] Xue H, Yang Y, Gao F, et al. Acoustic higher-order topological insulator on a kagome lattice. Nat Mater 2019;18:108–12.
- [40] Ni X, Weiner M, Alù A, et al. Observation of higher-order topological acoustic states protected by generalized chiral symmetry. Nat Mater 2019;18:113–20.
- [41] Zhang X, Wang HX, Lin ZK, et al. Second-order topology and multidimensional topological transitions in sonic crystals. Nat Phys 2019;15:582–8.
- [42] Peri V, Song ZD, Serra-Garcia M, et al. Experimental characterization of fragile topology in an acoustic metamaterial. Science 2020;367:797–800.
- topology in an acoustic metamaterial. Science 2020;367:797–800.

 [43] Qian K, Apigo DJ, Padavić K, et al. Observation of Majorana-like bound states in
- metamaterial-based Kitaev chain analogs. Phys Rev Research 2023;5:L012012.
 [44] He QL, Pan L, Stern AL, et al. Chiral Majorana fermion modes in a quantum anomalous Hall insulator-superconductor structure. Science 2017;357:294–9.
- [45] Barlas Y, Prodan E. Topological classification table implemented with classical passive metamaterials. Phys Rev B 2018;98:094310.
- [46] Prodan E, Schulz-Baldes H. Bulk and Boundary invariants for Complex Topological Insulators: From *K*-Theory to Physics. Cham: Springer; 2016.
- [47] Liu Y, Liu Y, Prodan E. Braiding flux-tubes in topological quantum and classical lattice models from class-D. Ann Phys 2020;414:168089.
- [48] Barlas Y, Prodan E. Topological braiding of non-Abelian midgap defects in classical metamaterials. Phys Rev Lett 2020;124:146801.
- [49] Gao P, Torrent D, Cervera F, et al. Majorana-like zero modes in Kekulé distorted sonic lattices. Phys Rev Lett 2019;123:196601.
- [50] Chen CW, Lera N, Chaunsali R, et al. Mechanical analogue of a Majorana bound state. Adv Mater 2019;31:1904386.
- [51] Noh J, Schuster T, Iadecola T, et al. Braiding photonic topological zero modes. Nat Phys 2020;16:989–93.
- [52] Menssen AJ, Guan J, Felce D, et al. Photonic topological mode bound to a vortex. Phys Rev Lett 2020;125:117401.
- [53] Gao X, Yang L, Lin H, et al. Dirac-vortex topological cavities. Nat Nanotechnol 2020;15:1012–8.
- [54] Ma J, Xi X, Li Y, et al. Nanomechanical topological insulators with an auxiliary orbital degree of freedom. Nat Nanotechnol 2021;16:576–83.



Shi-Qiao Wu received his Ph.D. degree in Physical Electronics from South China University of Technology in 2018. Subsequenctly, he was a postdoctoral fellow at Hong Kong Baptist University and Soochow University. Since June in 2023, he has been a member of the School of Physics and Optoelectronics Engineering in Foshan University. His current research interest includes topological phononics and non-Hermitian topology.



Wenting Cheng earned her Ph.D. degree in Materials Science and Engineering from the New Jersey Institute of Technology in 2022, and currently, she is a postdoctoral researcher at the Physics Department, the University of Michigan. Her research focuses on exploring vibration modes and energy dispersion in classical metamaterials.



Emil Prodan received his Ph.D. degree in Theoretical and Computational Physics from Rice University in 2003. He also received postdoctoral training at University of California in Santa Barbara under the mentorship of Walter Kohn and at Princeton University under the mentorship of Duncan Haldane and Roberto Car. In 2007, he joined the Physics Department of Yeshiva University in New York, where he is currently a full professor. His research specialization is in mathematical physics and his research interests are in topological dynamics, both classical and quantum.



Camelia Prodan received her Ph.D. degree in Physics from University of Houston and continued with post-doctoral studies in the Physics Department at University of California in Santa Barbara. She is currently the Kim B. and Stephen E. Bepler Professor in Physics at Fordham University. Her research focuses on studying topological vibrational modes in meta materials and biological systems.



Jian-Hua Jiang received his Ph.D. degree in Condensed Matter Physics from the University of Science and Technology of China in 2010. He was a post-doctoral fellow at the Weizmann Institute of Science under the supervision of Yoseph Imry, and later at the University of Toronto under the supervision of Sajeev John. In 2015, he joined Soochow University as full professor of physics. In 2023, he joined the University of Science and Technology of China as full professor of physics. His research focuses on materials physics and nonequilibrium physics, with particular interests in materials innovations, topological physics, and emergent collective phenomena